JCTC Journal of Chemical Theory and Computation

Theoretical Study of Binding Site Preference in [2]Rotaxanes

Michael E. Foster and Karl Sohlberg*

Department of Chemistry, Drexel University, 3141 Chestnut Street, Philadelphia, Pennsylvania 19104

Received June 28, 2007

Abstract: Rotaxanes that can be switched between co-conformations by some external stimulus are of interest because the switching mechanism might be used to create molecular devices capable of producing useful work. Probably the most common approach to create a switchable rotaxane is to start with a rotaxane where the ring interacts more strongly with one of two possible binding sites along the shaft and then apply an external stimulus that weakens the binding interaction between the ring and the shaft at this site, thereby changing the binding site preference. We have investigated binding site preference in two rotaxanes and two pseudo-rotaxanes with electronic structure calculations at several levels of theory. To gain insight into the origins of the intercomponent binding, empirical approximations were applied to estimate the electrostatic and dispersion contributions. Dispersion has been thought to make an important contribution to the intercomponent interaction in the presence of $\pi-\pi$ stacking interactions between the components, but the role of dispersion interaction has been a controversial issue because many computational methods neglect this interaction. For example, AM1 semiempirical calculations neglect dispersion but often predict correct co-conformational preferences. This suggests that inclusion of the dispersion interaction is required for correct quantitative, but not qualitative, description of the intercomponent binding, a result that is supported by the analytic partitioning of the binding interactions. The origins of this result are investigated.

1. Introduction

In the search for molecular systems that can serve as functional components of mechanical nanodevices, switchable rotaxanes have become a center of focus.[1−3] A rotaxane is an interlocked molecular complex wherein a ring molecule is threaded by a long chain molecule. The long chain molecule is terminated with bulky functional groups that have larger radii than the internal diameter of the ring, preventing spontaneous ring unthreading. In a [2]rotaxane therefore, the two component molecules are mechanically linked but chemically independent. A *switchable* rotaxane is a rotaxane that can be switched between two co-conformational isomers through the application of an external stimulus. Switchable rotaxanes are therefore of special interest because they contain the essential features of a molecular "machine" or "device," and mechanical action is accomplished through the application of an external stimulus.

To facilitate the design of nanodevices based on switchable rotaxanes, it would be of great value to identify a robust and efficient theoretical modeling technique. Numerous approaches have been explored.[4,5] One technique that has shown considerable success is AM1[6] semiempirical electronic structure methodology. Semiempirical electronic structure calculations have at least two desirable features. First, they are computationally efficient (relative to ab initio approaches) and therefore may be routinely used on systems of the size of interlocked macromolecular complexes. Second, semiempirical methods explicitly describe the electronic structure and therefore may be used on various charge and electronic states of a system without reparametrization. This second advantage is especially valuable for switchable rotaxanes, because many proposed switching mechanisms depend on a

* Corresponding author e-mail: sohlbergk@drexel.edu.

10.1021/ct7001623 CCC: $37.00
Published on Web 10/18/2007

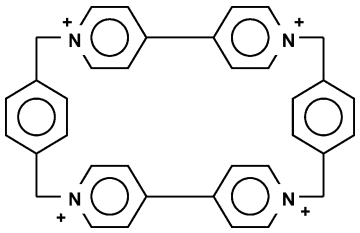

Figure 1. Tetracationic ring structure used in all rotaxane and pseudorotaxane systems considered here.

change in the charge or electronic state of the system. An alternative approach would be to employ molecular mechanics (MM) methods, which are also computationally efficient. MM methods, however, typically require reparametrization to treat different charge states, in particular the assignment of partial atomic charges. Such partial charges are often obtained by first carrying out semiempirical or ab initio electronic structure calculations on the same or a closely related system,[7] which partially negates the advantages of the MM methods. Since atomic partial charges vary with molecular conformation,[8] one must either carry out true electronic structure calculations for multiple conformations to establish this structure dependence or employ an empirical approach to assign them dynamically.[9] Since MM calculations do not yield explicit electronic structure information, they are also not generally applicable to obtain molecular orbital information or for modeling excited electronic states.

One of the key features that a modeling technique must predict reliably to be valuable as a tool for the design of switchable interlocked macromolecular systems is co-conformational selectivity. Selectivity is determined by the intercomponent nonbonding interactions.[10−13] Since the AM1 Hamiltonian produces qualitatively correct ordering of hydrogen-bonding interactions,[14] it may be confidently used to predict co-conformational selectivity in interlocked macromolecular complexes where hydrogen-bonding dominates the intercomponent interactions. Several rotaxanes and catenanes systems of this nature have been studied with success utilizing the AM1 method.[5,15,16] In many switchable rotaxanes, however, the dominant intercomponent interaction is $\pi-\pi$ stacking, which is governed by dispersion forces. Since AM1 is a HF-based technique, it neglects dispersion. One might expect, therefore, AM1 to be unreliable in application to such systems, but, remarkably, it has proven to be unexpectedly successful in this role, as shown in the present manuscript and elsewhere.[17] It is therefore of considerable importance to understand the limits of reliability of the semiempirical methods. We aim to better characterize the range of applicability of the semiempirical AM1 method, in general, and to understand in particular why AM1 is qualitatively successful in predicting binding site preference in $\pi-\pi$ stacked interlocked macromolecular complexes despite its neglect of dispersion.

In this manuscript we report electronic structure calculations at several levels of theory on several rotaxane and pseudorotaxane systems. All of these systems incorporate the same ring structure (shown in Figure 1). The different shaft structures are shown in Figures 2 and 3. To gain further insight into the interactions between the two components, empirical approximations to the electrostatic and dispersion interactions were also used. The results suggest an origin of the unexpected "success" of AM1 for modeling $\pi-\pi$ stacked interlocked macromolecular complexes.

2. Theoretical Methods

2.1. Electronic Structure Calculations. The interlocked macromolecular systems studied here contain from 92 to 242 atoms. The cyclobis(paraquat-*p*-phenylene) ring, used in all of the systems, contains 72 atoms. Determining the electronic structure of systems of this size presents a very considerable computational challenge. Because of their computational efficiency, semiempirical electronic structure methods hold promise in this application. We therefore seek to identify the limits of their applicability. Since it is widely accepted to be one of the most robust semiempirical methods, herein we explore the application of the AM1 Hamiltonian.[6]

To calibrate the accuracy of the AM1 calculations and to gain insight into the intercomponent interactions, Hartree−Fock self-consistent-field (HF-SCF) calculations and density functional theory (DFT) calculations, based on the B3LYP correlation-exchange functional, were carried out on a subset of the systems studied here. Various orbital basis sets were employed for the wave function expansion to test for convergence with respect to basis set completeness and to assess the sensitivity of the predicted intercomponent interactions to basis set size. In the HF-SCF and DFT calculations of the intercomponent interaction energies, the counterpoise (CP) correction to the basis set superposition error (BSSE) was determined as follows

$$\mathrm{CP} = (E_s^{sp'} - E_s^{sp}) + (E_r^{sp'} - E_r^{sp}) \qquad (1)$$

where E_r^{sp} and E_s^{sp} are the single-point energies of the ring and shaft in the rotaxane geometry, and $E_r^{sp'}$ and $E_s^{sp'}$ are the single-point energies of the ring and shaft in the rotaxane geometry using the rotaxane basis. It is important to note

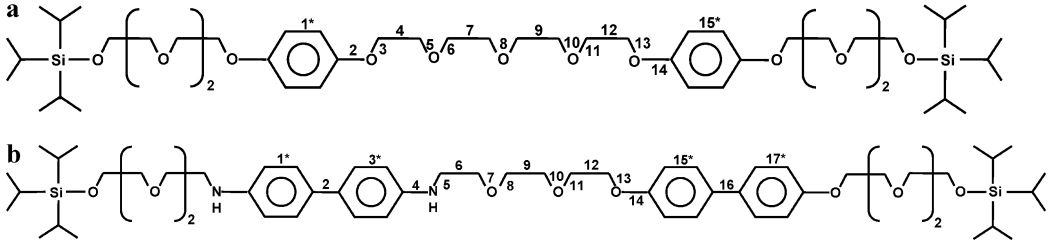

Figure 2. Top - rotaxane **1** shaft, bottom - rotaxane **2** shaft. The numbers on the shafts (a and b) correspond to the bond numbers in the appropriate figures.

that the presence of BSSE results in an overestimation of the interaction energy; therefore, the value obtained from eq 1 reduces the binding energy.

All electronic structure calculations were carried out in delocalized internal coordinates as implemented in the GAMESS suite of codes.[18]

2.2. Empirical Approximations. Empirical approximations were used to gain further insight into the electrostatic and dispersion contributions to the interactions between the components in the rotaxanes and pseudorotaxanes. The two different approximations are discussed and shown in algebraic form below.

2.2.1. Electrostatic Interactions. The electrostatic interactions were approximated by assuming a Coulomb interaction of atomic point charges by employing the following equation

$$E_{\text{electrostatic}} = \sum_{i_{\text{RING}}} \sum_{j_{\text{SHAFT}}} \frac{Q_i Q_j}{r_{ij}} \tag{2}$$

where Q_i, Q_j, and r_{ij} are the net charge of an atom on the cyclophane ring, the net charge of an atom on the shaft, and the distance between these atoms, respectively. The net charges on each atom were taken to be the MOPAC charges from the AM1 calculations. The distances between the atoms were obtained from the corresponding AM1 optimized structure. It should be noted that since real atoms are not point charges, the equation is only approximate and works best in the long-range limit.

2.2.2. Dispersion Interactions. The dispersion interaction was estimated by employing an empirical approximation set forth by Grimme[19]

$$E_{\text{dispersion}} = -s \sum_{i_{\text{RING}}} \sum_{j_{\text{SHAFT}}} \frac{\sqrt{C^i C^j}}{r_{ij}^{\,6}} \left(\frac{1}{1 + \mathrm{e}^{-d(r_{ij}/R-1)}} \right) \tag{3}$$

where C_i and C_j are dispersion coefficients corresponding to the element; r_{ij} and R are the distance between the two atoms and the sum of the atomic vdW radii, respectively; and S and d are scaling factors as reported by Grimme.[19] The equation was validated by applying it to several dimer systems with well-known dispersion interactions as presented in the Results section below.

2.3. Model Building. In order to generate reasonable starting structures for the AM1 calculations, partial optimizations of the components and the complexes were carried out using molecular mechanics (MM) methods with the AMBER force field.[20] It is important to note that MM was only used to generate starting structures not for final optimizations or energy calculations. All Graphical model building and preliminary partial optimizations were carried out with the Hyperchem software package.[21] Molekel advanced 3D-molecular graphics was used for viewing and to create the images provided herein.[22]

3. Computational Methods

The stating structures of the rotaxanes and pseudorotaxanes were obtained by first constructing the ring and shafts separately. The different components were built with a graphical-user-interface molecular editor and partially optimized using molecular mechanics (AMBER force field) to obtain reasonable component starting structures. The separate components were then each fully optimized at the AM1 level. The fully optimized components were then manually assembled into full complexes with a GUI molecular editor, centering the ring about the shaft slightly offset from a binding site. These interlocked structures were again partially optimized using MM to eliminate any close contacts. Finally, the full interlocked structures were fully optimized at the AM1 level. Difficulties in obtaining SCF convergence in the rotaxane structures were overcome by displacing the ring about the shaft in small steps until convergence could be achieved.

Once an optimized rotaxane was obtained, an effective potential energy curve (shuttling barrier) for translation of the ring along the shaft was obtained by mapping the potential energy at the AM1 level of theory with a series of restrained optimizations. Restraints were applied between the ring and the shaft so as to fix the position of the ring relative to specific atoms on the shaft. A set of optimized structures (with restraints) was generated for each position of the ring along the shaft between the two binding sites. At each position along the shaft, the ring was rotated by a random angle about the shaft and reoptimized. The new optimized coordinates were used for the subsequent rotation, and the process was repeated on average 10 times (not all optimizations converged). In some cases the SCF procedure failed to converge, typically because the starting structure that was autogenerated by our rotation procedure was unphysical. These unphysical structures were discarded. After performing constrained optimizations for each position of the ring along the shaft, the structures generated were regrouped by identifying the bond along the shaft to which the centroid of the ring was closest. (This was not always the bond to which the ring was constrained, due to the freedom of movement the remainder of the structure.) A Boltzmann-weighted average energy was obtained for each position of the ring along the shaft. A total of 165 structures was generated and optimized for rotaxane **1**, with a minimum of 5 and a maximum of 36 structures per position about the shaft. One hundred ninety-four structures were generated and optimized for rotaxane **2**, with a minimum of 4 and a maximum of 42 structures per position. The shaft of rotaxane **1** has symmetric connectivity about its midpoint; therefore, the symmetric bond positions were combined for analysis.

For pseudorotaxane **3** (pseudoshaft a) the PEC was mapped in a slightly different manner. The system was built and optimized in the same manner as the rotaxanes. Following Grabuleda and Jaime,[12] the ring was thrice shuttled back and forth along the shaft in a stepwise manner and restrained to specific atoms on the shaft at each step (no rotations of the ring about the shaft were preformed). The same approach was used to determine the closest bond along the shaft to the center of the ring as in the rotaxane systems. A total of 39 structures were generated by the shuttling process. Pseudoshaft a (Figure 3) also has symmetric connectivity about its midpoint allowing symmetric positions to be combined for analysis. As for the rotaxane systems, a

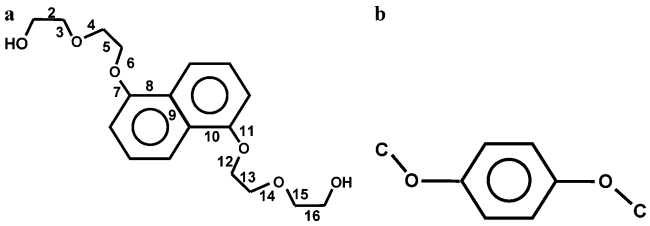

Figure 3. Left - pseudorotaxane **3** shaft, right - pseudorotaxane **4** shaft. The numbers on shaft (a) correspond to the bond numbers in the appropriate figures.

Boltzmann average was again taken of the set of energy values obtained at each position.

For pseudorotaxane **3**, the PEC for ring shuttling along the shaft was also mapped at the HF-SCF level. HF optimizations were performed on the lowest energy structures from each set as identified by the AM1 calculations, applying the same restraints to hold the ring in position. The HF calculations allowed for the BSSE to be determined by performing CP-correction calculations.

Pseudorotaxane **4** contains a very short shaft; therefore, the system was only studied in one relative position (associated). As in the other cases, the shaft was first optimized at the AM1 level and then manually associated with the optimized ring, and the entire complex was fully optimized. Full optimizations were also performed at the HF and DFT levels using the 6-31G(d) basis. In addition, single-point calculations at the HF-SCF level, using various basis sets, were performed on the different optimized structural geometries. CP-correction calculations were performed for all first-principles calculations.

To calibrate the reliability of the empirical dispersion expression (eq 3), four different dimer systems were studied: hydrogen, nitrogen, water, and nitromethane. The dispersion interaction values and reported geometries were found in the following references: hydrogen,[23] nitrogen,[24] water,[25] and nitromethane.[26,27] The reported geometries were used to determine the distances between the atoms of the two monomers as required for application of eq 3.

The water and nitromethane dimers were further studied to examine the consequences of performing single-point calculations on structures resulting from optimizations carried out at a different level of theory. These systems were fully optimized at the AMBER, AM1, HF/6-31G(d), B3LYP/6-31G(d), and B3LYP/6-311G(dp) levels; the water dimer was also optimized at the MP2/6-31G(d,p) level. As in the case of pseudorotaxane **4**, single-point calculations at the HF-SCF level, using various basis sets, were performed on the different optimized structural geometries. All of the calculations were CP-corrected. The results are presented and discussed below.

4. Results

4.1. Rotaxane 1. The shuttling barrier for movement of the ring between the two identical hydroquinone binding stations on the shaft of rotaxane **1** is shown in Figure 4. (A schematic of the shaft is shown in Figure 2a.) The AM1 PEC (Figure 4) shows that the ring preferentially lies at one of the equivalent binding stations. The lowest energy structure

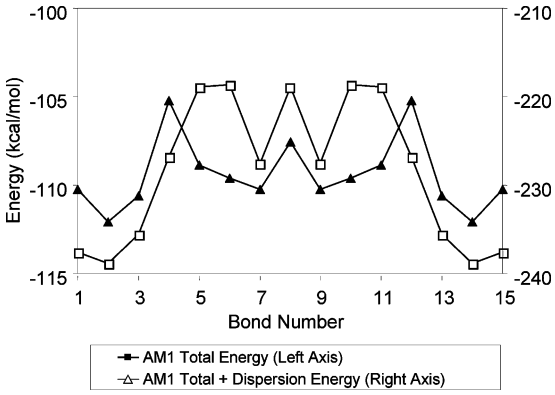

Figure 4. AM1 total energy and AM1 total energy plus dispersion energy for the shuttling process in rotaxane **1**. The bond numbers correspond to the number on the shaft as shown in Figure 2a.

obtained from the AM1 method is shown in Figure 5. The energy required for the ring to move from one station to the other was determined to be 10.1 kcal/mol. This is in good agreement with computational results obtained by Grabuleda and Jaime,[12] where they determined the barrier to be 10.8 kcal/mol using molecular mechanics (MM3 force field) simulations. These results are in relatively good agreement with the experimental result of 13 kcal/mol obtained by Anelli.[28] It is important to note that the computational values from the literature and our own AM1 values differ from the corresponding experimental results by less than the standard error in calculations of their type.[29] In other words, the differences are not statistically significant.

Since van der Waals (dispersion) interactions are neglected in the AM1 method, eq 3 was used to estimate the magnitude of this interaction between the two components. The PEC with the empirical estimate of the dispersion interaction added to the AM1 binding energy is shown in Figure 4. The same preferred binding site is predicted as from the AM1 results alone. With the inclusion of the dispersion interaction, the shuttling barrier is 13.7 kcal/mol. Since the MM calculations of Grabuleda and Jaime[12] considered dispersion interactions, it is most appropriate to compare their result to our AM1 result with the inclusion of dispersion. In this case our result is indeed closer to the experimental value of 13 kcal/mol, although the difference is again not statistically meaningful.

The electrostatic interaction between the components as the ring is moved along the shaft as estimated using eq 2 is shown graphically in Figure 6. The electrostatic interaction also predicts the ring to lie preferentially at one of the equivalent binding sites. Note that the electrostatic energy as estimated with the Coulomb expression (eq 2) and the MOPAC point-charge approximation (obtained form the AM1 calculations) predicts qualitatively the same binding site preference as the AM1 calculation.

4.2. Rotaxane 2. The barrier to ring-shuttling in rotaxane **2** was mapped in a similar manner as for rotaxane **1**. The resulting PEC based on AM1 with/without inclusion of dispersion is shown in Figure 7. Rotaxane **2** contains benzidine and 4,4′-biphenol binding stations; a schematic of the shaft is shown in Figure 2b. The ring is predicted to reside

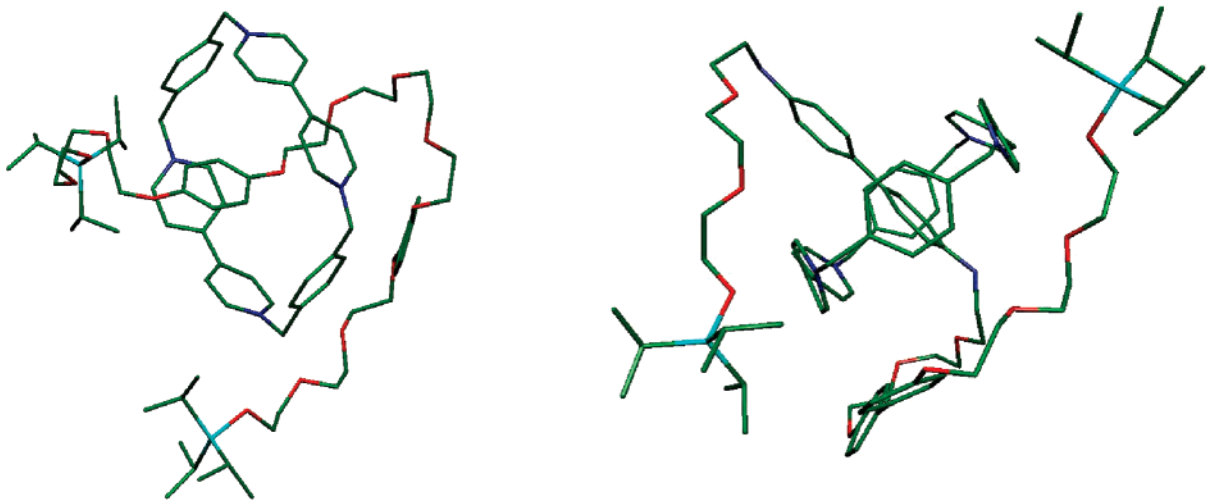

Figure 5. AM1 fully optimized structures of [2]rotaxane **1** (shaft **a**) on the left and [2]rotaxane **2** (shaft **b**) on the right.

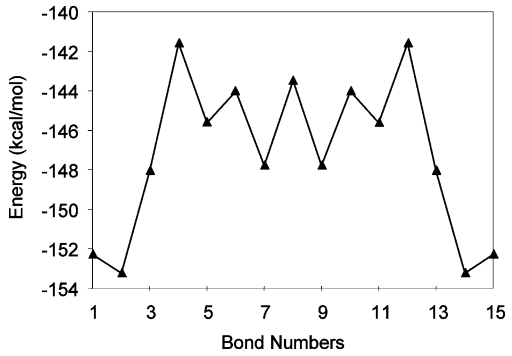

Figure 6. Electrostatic interaction energy between the ring and shaft in rotaxane **1** as calculated with eq 2.

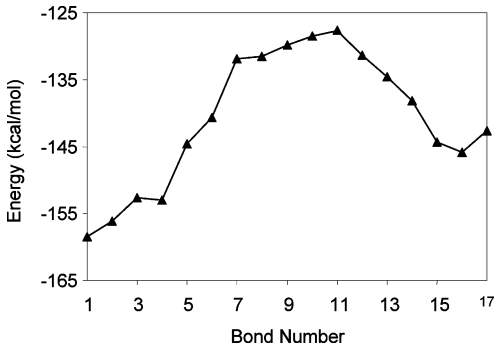

Figure 8. Electrostatic interaction energy between the ring and shaft in rotaxane **2** as calculated with eq 2.

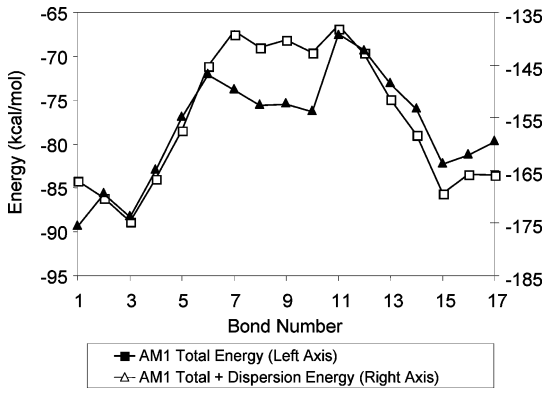

Figure 7. AM1 binding energy and AM1 binding energy plus dispersion energy for the shuttling process in rotaxane **2**. The bond numbers correspond to the number on the shaft as shown in Figure 2b.

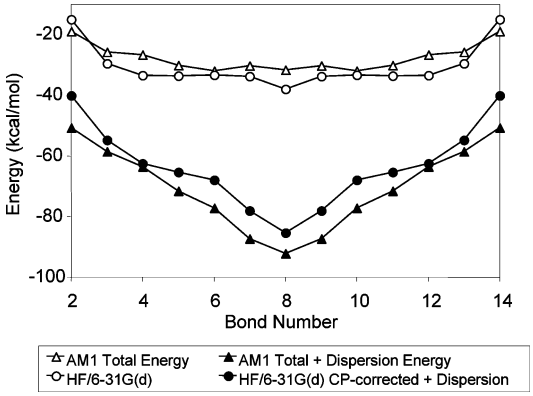

Figure 9. Upper curves - AM1 binding energy and AM1 binding energy plus dispersion energy for the shuttling process in pseudorotaxane **3**. The bond numbers correspond to the number on the shaft as shown in Figure 3a. Lower curves - HF/6-31G(d) binding energy and HF/6-31G(d) binding energy plus dispersion energy of pseudorotaxane **3** as a function of bond number (shown in Figure 3a).

preferentially at the benzidine station both with and without the dispersion contribution included. The predicted binding site preference is in agreement with experimental data.[30] The benzidine station was found to be favored by 3.2 kcal/mol at the AM1 level and by 11.9 kcal/mol when the dispersion interaction was included. A Boltzmann distribution based on either result reveals that the ring resides at the benzidine site virtually 100% of the time at 300 K. The lowest energy structure obtained from the AM1 calculations is shown in Figure 5, where it can be seen how the ring orients relative to the benzidine station. The electrostatic interaction energy, as calculated using the empirical eq 2 for various positions of the ring relative to the shaft, is shown in Figure 8. As for rotaxane **1**, The electrostatic interaction predicts the same preferred binding site (benzidine).

In this [2]rotaxane system, the two binding sites are nonidentical. This provides the opportunity to control the

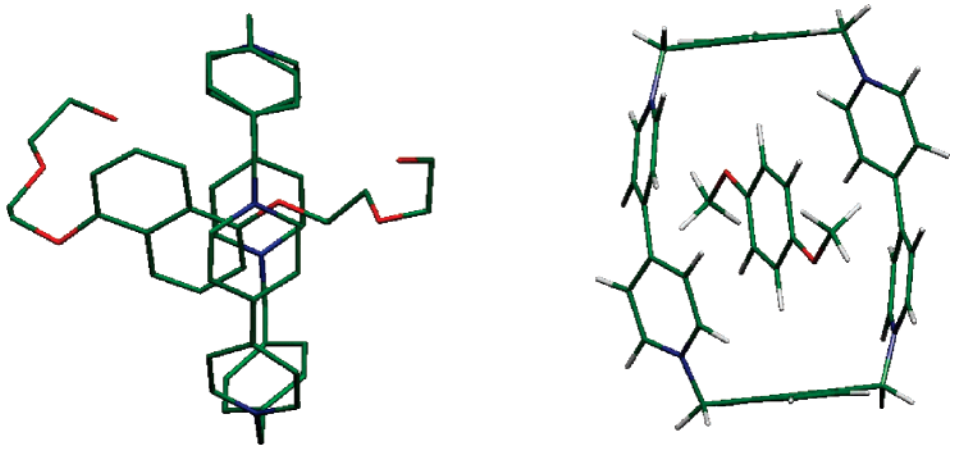

Figure 10. AM1 fully optimized structures of [2]pseudorotaxane **3** (shaft **c**) on the left and [2]pseudorotaxane **4** (shaft **d**) on the right.

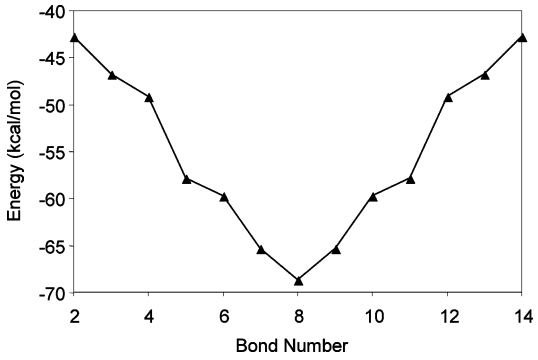

Figure 11. Electrostatic interaction energy between the ring and shaft in pseudorotaxane **3** as calculated with eq 2.

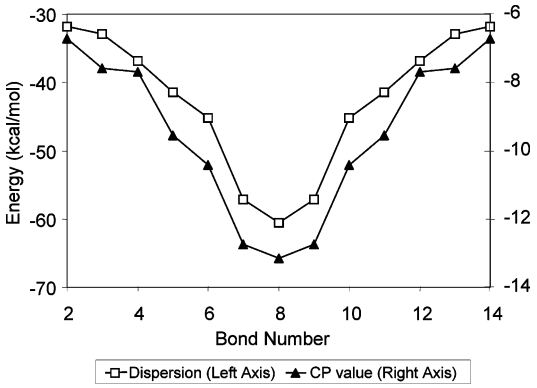

Figure 12. CP-correction energy and dispersion interaction energy as a function of the bond number (shown in Figure 3a) for pseudorotaxane **3**. Note that while the magnitudes differ significantly (the scales on the left and right vertical axes differ), qualitatively the CP correction tracks the dispersion energy very closely.

binding site preference by some external stimulus. Upon oxidation of this system, the benzidine station becomes positively charged, repelling the tetracationic ring to the 4,4′-biphenol station. This has been shown to occur experimentally by Bissell et al.[31] Semiempirical AM1 electronic structure calculations indeed show a very strong repulsion of the ring from the positively charged benzidine site when the system is in its oxidized state, resulting in restabilization of the ring around the 4,4′-biphenol station.

4.3. Pseudorotaxane 3. A schematic of the shaft of pseudorotaxane **3** is shown in Figure 3a. This system contains a 1,5-dioxynaphthalene binding station. Potential energy curves were generated for movement of the tetracationic ring relative to this shaft using both the AM1 and HF-SCF methods. The AM1 PEC with/without the inclusion of the empirical dispersion term is shown in Figure 9. This figure shows that the lowest energy structure corresponds to the ring positioned at the binding station (AM1 optimized structure, Figure 10). The electrostatic interaction as estimated with eq 2 also predicts the ring to bind at the 1,5-dioxynaphthalene binding station. The variation in the electrostatic interaction as the ring is shuttled along the shaft is shown in Figure 11. The geometries used for these electrostatic interaction calculations were obtained from the AM1 calculations.

To further investigate the root of the intercomponent binding, HF/6-31G(d) optimizations were carried out starting from the lowest energy AM1 structures at each position of the ring along the shaft. The PEC at the HF level of theory is shown in Figure 9. This figure also shows the CP-corrected HF energy plus the calculated empirical dispersion contribution. Both cases predict the ring to lie preferentially at the binding station. Note also the striking similarity between the AM1 and HF results.

Table 1. Calculated Binding Energies of Pseudorotaxane **4** Resulting from Full Optimizations at the AM1, HF/6-31G(d), and DFT/6-31G(d) Levels of Theory[a]

	AM1	HF/6-31G(d)	B3LYP/6-31G(d)
ring	−214.42887	−1598.46148	−1607.77949
sp. ring w/ring basis	N/A	−1598.40103	−1607.77831
sp. ring w/system basis	N/A	−1598.40599	−1607.78329
SHAFT	−66.22266	−458.45968	−461.01456
sp. shaft w/ring basis	N/A	−458.45984	−461.01785
sp. shaft w/system basis	N/A	−458.46420	−461.02378
pseudorotaxane	−280.66075	−2056.93618	−2068.81641
Δ***E*** (kcal/mol)	−5.79	−9.43	−14.03
Δ***E*** CP-corrected (kcal/mol)	N/A	−3.58	−7.19

[a] Energies in hartrees except as otherwise noted.

Table 2. Raw SP Energies, Binding Energies, and CP-Correction Values for Pseudorotaxane **4** Based on Coordinates Obtained by Full Optimization at Four Different Levels of Theory

	HF/6-31G	HF/6-31G(d)	HF/6-31G(d,p)	HF/6-311G(d,p)	HF/6-311+G(d,p)
			AM1 Coordinates		
ring	−1597.79922	−1598.40285	−1598.46088	−1598.72567	−1598.73577
ring[a]	−1597.79746	−1598.40103	−1598.45902	−1598.72402	−1598.73405
ring[b]	−1597.80215	−1598.40599	−1598.46408	−1598.72682	−1598.73728
shaft	−458.26112	−458.44792	−458.46483	−458.55770	−458.56447
shaft[a]	−458.26137	−458.44766	−458.46460	−458.55750	−458.56428
shaft[b]	−458.26547	−458.45188	−458.46876	−458.56139	−458.56714
pseudorotaxane	−2056.07364	−2056.86277	−2056.93790	−2057.29364	−2057.30954
Δ*E* (kcal/mol)	−8.35	−7.53	−7.65	−6.45	−5.84
CP-correction (kcal/mol)	−5.51	−5.76	−5.79	−4.21	−3.82
Δ*E* CP-corrected (kcal/mol)	−2.84	−1.77	−1.86	−2.24	−2.02
			HF/6-31G(d) Coordinates		
ring	−1597.85461	−1598.46148	−1598.51854	−1598.78375	−1598.79347
ring[a]	−1597.85333	−1598.45998	−1598.51700	−1598.78254	−1598.79218
ring[b]	−1597.85788	−1598.46483	−1598.52196	−1598.78514	−1598.79523
shaft	−458.26971	−458.45968	−458.47628	−458.56935	−458.57617
shaft[a]	−458.27238	−458.45984	−458.47646	−458.56950	−458.57624
shaft[b]	−458.27653	−458.46420	−458.48082	−458.57337	−458.57901
pseudorotaxane	−2056.14286	−2056.93618	−2057.01003	−2057.36640	−2057.38170
Δ*E* (kcal/mol)	−11.63	−9.43	−9.54	−8.34	−7.57
CP-correction (kcal/mol)	−5.46	−5.78	−5.84	−4.06	−3.66
Δ*E* CP-corrected (kcal/mol)	−6.17	−3.65	−3.70	−4.28	−3.91
			B3LYP/6-31G(d) Coordinates		
ring	−1597.84630	−1598.44991	−1598.50706	−1598.77161	−1598.78146
ring[a]	−1597.84540	−1598.44895	−1598.50608	−1598.77075	−1598.78065
ring[b]	−1597.85002	−1598.45386	−1598.51109	−1598.77350	−1598.78376
shaft	−458.26870	−458.45630	−458.47303	−458.56592	−458.57278
shaft[a]	−458.27068	−458.45592	−458.47266	−458.56553	−458.57232
shaft[b]	−458.27544	−458.46092	−458.47764	−458.56997	−458.57524
pseudorotaxane	−2056.13369	−2056.92159	−2056.99566	−2057.35096	−2057.36600
Δ*E* (kcal/mol)	−11.73	−9.65	−9.78	−8.42	−7.38
CP-correction (kcal/mol)	−5.89	−6.22	−6.27	−4.51	−3.78
Δ*E* CP-corrected (kcal/mol)	−5.84	−3.43	−3.51	−3.91	−3.60
			Ercolani Coordinates B3LYP/6-31G(d,p)		
ring	−1597.84745	−1598.45117	−1598.50832	−1598.77284	−1598.78273
ring[a]	−1597.84636	−1598.44996	−1598.50709	−1598.77178	−1598.78168
ring[b]	−1597.85099	−1598.45488	−1598.51210	−1598.77454	−1598.78482
shaft	−458.27057	−458.45732	−458.47404	−458.56689	−458.57363
shaft[a]	−458.27089	−458.45611	−458.47284	−456.17202	−458.57249
shaft[b]	−458.27573	−458.46117	−458.47789	−456.17545	−458.57542
pseudorotaxane	−2056.13489	−2056.92276	−2056.99681	−2057.35213	−2057.36710
Δ*E* (kcal/mol)	−10.58	−8.95	−9.07	−7.78	−6.73
CP-correction (kcal/mol)	−5.94	−6.27	−6.31	−3.88	−3.82
Δ*E* CP-corrected (kcal/mol)	−4.64	−2.69	−2.76	−3.90	−2.92

[a] Ring/shaft energy in system geometry with ring/shaft basis. [b] Ring/shaft energy in system geometry with pseudorotaxane basis. Energies in hartrees except as otherwise noted. Ercolani's coordinates can be found in ref 32.

To provoke a discussion of why calculations that neglect dispersion predict the correct binding site preference, a graph of the dispersion interaction (as obtained from the empirical eq 3 using the AM1 optimized geometries) and the CP-correction values (HF-SCF calculations) is shown in Figure 12. While the magnitudes differ significantly (note the different energy scales on the left and right vertical axes of Figure 12), this figure shows that the CP-correction qualitatively tracks the dispersion interaction very closely.

4.4. Pseudorotaxane 4. As mentioned earlier, pseudorotaxane **4** was only studied in one relative position (associated). The smaller size of this system allowed higher order calculations to be performed. The system and its components were optimized at the AM1, HF/6-31G(d), and DFT/6-31G(d) levels of theory, with the HF and DFT calculations being CP-corrected. The energy of the system and each component as well as the calculated binding energies are reported in Table 1. The effect of performing single-point calculations on structure geometries obtained at another level of theory was then investigated. Such comparisons are shown in Tables 2 and 3. In Table 2, four optimized geometries (AM1, HF/6-31G(d), B3LYP/6-31G(d), and coordinates

Table 3. Effect of Performing Single-Point Calculations on Pseudorotaxane **4** at Different Optimized Geometries[a]

	system	ring	shaft
AM1	−280.66075	−214.42887	−66.22266
AM1//HF/6-31G*	−280.57939	−214.36381	−66.20724
energy difference (kcal/mol)	−51.05	−40.83	−9.68
AM1	−280.66075	−214.42887	−66.22266
AM1//B3LYP/6-31G*	−280.62485	−214.40041	−66.21672
energy difference (kcal/mol)	−22.53	−17.86	−3.73
HF/6-31G*	−2056.93618	−1598.46148	−458.45968
HF/6-31G*//B3LYP/6-31G*	−2056.92159	−1598.44991	−458.45630
energy difference (kcal/mol)	−9.16	−7.26	−2.12
B3LYP/6-31G(d)	−2068.81641	−1607.77949	−461.01456
B3LYP/6-31G(d)//HF/6-31G(d)	−2068.80261	−1607.76882	−461.01141
energy difference (kcal/mol)	−8.66	−6.70	−1.97

[a] Energies in hartrees except as otherwise noted.

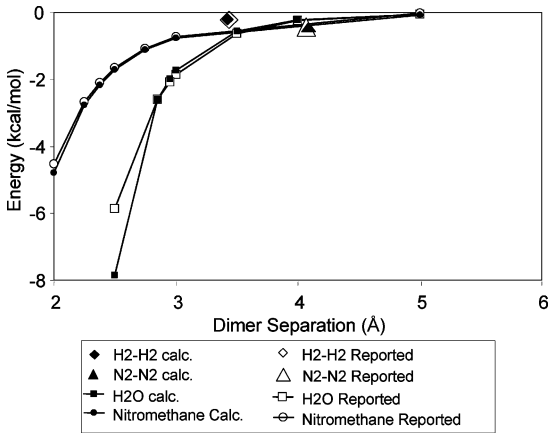

Figure 13. Dispersion interaction energy in the hydrogen, nitrogen, water, and nitromethane dimers as calculated using the empirical approximation of Grimme[19] with comparison to accurate values from the literature: $(H_2)_2$,[23] $(N_2)_2$,[24] $(H_2O)_2$,[25] $(CH_3NO_2)_2$.[26,27]

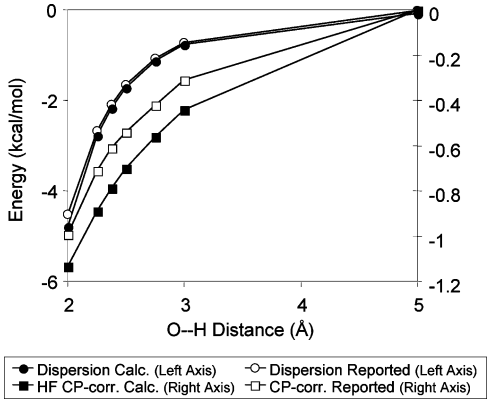

Figure 14. Dispersion interactions and CP correction as a function of the nitromethane dimer separation as calculated using the empirical approximation of Grimme[19] with comparison to accurate values from the literature.[26,27]

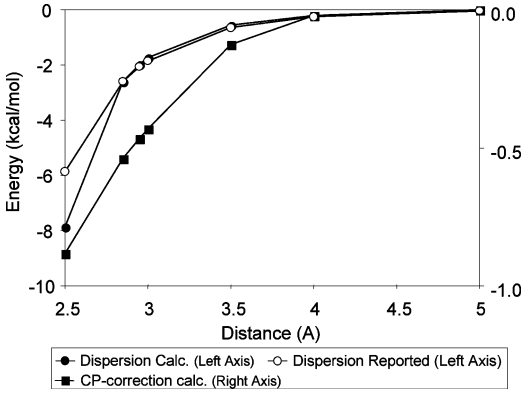

Figure 15. Dispersion interactions and CP correction as a function of the water dimer separation as calculated using the empirical approximation of Grimme[19] with comparison to accurate values from the literature.[25]

reported by Ercolani and Mencarelli,[32] who used the B3LYP/6-31g(d,p) method) were subjected to single-point calculations using various basis sets at the HF-SCF level: HF/6-31G, HF/6-31G(d), HF/6-31G(d,p), HF/6-311G(d,p), and HF/6-311+G(d,p). From these data, the difference in energy between a calculation on a fully optimized structure and single-point calculations based on structures obtained from optimization at a different level of theory may be determined. As shown in Table 3, this energy difference typically exceeds the binding energy of the complex. In the most extreme case the energy difference is 51 kcal/mol. This large shift is potentially critical as will be discussed later.

4.5. Dimer Systems. To validate the empirical dispersion expression due to Grimme,[19] Figure 13 compares the *inter*component dispersion interaction for four dimer systems (hydrogen, nitrogen, water, and nitromethane) as calculated by eq 3 with accurate values from the literature. For the $(H_2)_2$[23] and $(N_2)_2$[24] systems, the experimental binding energy is taken to be the "correct" value of the dispersion interaction since the intermonomer interaction is essentially pure dispersion in these cases. For the water[25] and nitromethane[26,27] dimers, accurate dispersion interaction energies were taken from SAPT calculations in the cited references. These results suggest that this empirical dispersion expression will predict with good accuracy the dispersion interaction between the ring and the shaft, as long as there are no close contacts, a condition that is expected to be fulfilled in the present case, i.e., *inter*component interactions in nonbonded rotaxane and pseudorotaxane complexes.

To help better understand the different contributions to intercomponent binding in the rotaxane and pseudorotaxane systems, several different types of calculations were performed on the water and nitromethane dimers. Single-point calculations (CP-corrected) were carried out at the HF/6-31G(d) level based on previously reported[25−27] dimer and monomer geometries. Figure 14 shows a graph of the calculated CP-correction, and dispersion interaction as estimated with eq 3, as a function of nitromethane dimer separation and compares these to accurate values from the literature (from refs 26 and 27). Figure 15 shows the same information for the water dimer; however, no CP-correction values were found in the literature for comparison. The

Table 4. Binding Energies of the Nitromethane Dimer at Different Level Theory (Optimized Calculations)[a]

	AM1	HF/6-31G(d)	B3LYP/6-31G(d)
monomer	−37.27434	−243.66198	−244.89022
dimer	−74.55654	−487.33076	−489.78855
Δ***E*** (kcal/mol)	−4.93	−4.26	−5.09
Δ***E*** CP-corrected (kcal/mol)	N/A	−3.46	−3.21

[a] Energies in hartrees except as otherwise noted.

reported dispersion interaction energies for the various geometries were obtained from refs 33 and 25. In both the water and nitromethane cases, the CP-correction qualitatively tracks the dispersion interaction, although it is quantitatively smaller. This tracking is similar to the result obtained for pseudorotaxane **3**.

Further calculations were undertaken to determine the consequences of performing SP calculations using structures optimized with a different level of theory and to explore the degree to which the calculations are converged with respect to basis set completeness. The water and nitromethane dimer systems were optimized at the AM1, HF/6-31G(d), and B3LYP/6-31G(d) levels, and the intercomponent binding energies were determined for comparison. The water dimer was also optimized at the MP2/6-31G(d,p) level. The calculated binding energies for nitromethane and water, both with and without CP-correction, are reported in Tables 4 and 6, respectively. The several optimized geometries were then subjected to single-point calculations using various basis sets at the HF-SCF level: HF/6-31G, HF/6-31G(d), HF/6-31G(d,p), HF/6-311G(d,p), and HF/6-311+G(d,p). The intercomponent interaction energies at the different levels of theory, for the nitromethane and water dimers, are tabulated in Tables 5 and 7, respectively.

To assess the reliability of structures obtained by performing optimization with a different level of theory, single-point calculations were carried out at the B3LYP/6-311G(dp) level on optimized geometries of the water and nitromethane dimers obtained at different levels of theory: AMBER, AM1, and HF/6-31G(d). Highly accurate published geometries of the water[25] and nitromethane[26,27] dimers were also considered. In Table 8, the total energies (B3LYP/6-311G(dp) single-point calculations) of the different dimer structures are reported. Since the literature geometries are assumed to be the most accurate, the absolute energy differences between the energy of the best published structure and that obtained at each other level of theory was calculated. The largest magnitude difference therefore corresponds to the least

Table 5. Binding Energies of the Nitromethane Dimer Based on Coordinates Obtained by Full Optimization at Four Different Levels of Theory

	HF/6-31G	HF/6-31G(d)	HF/6-31G(d,p)	HF/6-311G(d,p)	HF/6-311+G(d,p)
			AM1 Coordinates		
monomer	−243.52022	−243.65669	−243.66170	−243.72443	−243.73118
monomer A[a]	−243.51984	−243.65606	−243.66109	−243.72377	−243.73055
monomer A[b]	−243.52064	−243.65675	−243.66179	−243.72456	−243.73090
monomer B[a]	−243.51983	−243.65607	−243.66109	−243.72377	−243.73055
monomer B[b]	−243.52065	−243.65675	−243.66179	−243.72456	−243.73090
dimer (hartree)	−487.04999	−487.31917	−487.32954	−487.45532	−487.46795
Δ*E* (kcal/mol)	−6.00	−3.63	−3.85	−4.06	−3.52
CP-correction (kcal/mol)	−1.01	−0.86	−0.88	−0.99	−0.43
Δ*E* CP-corrected (kcal/mol)	−4.99	−2.77	−2.97	−3.07	−3.08
			HF/6-31G(d) Coordinates		
monomer	−243.52336	−243.66198	−243.66688	−243.72983	−243.73633
monomer A[a]	−243.52349	−243.66190	−243.66680	−243.72972	−243.73626
monomer A[b]	−243.52423	−243.66254	−243.66744	−243.73038	−243.73654
monomer B[a]	−243.52349	−243.66190	−243.66680	−243.72972	−243.73626
monomer B[b]	−243.52422	−243.66254	−243.66744	−243.73038	−243.73654
dimer (hartree)	−487.05615	−487.33076	−487.34075	−487.46683	−487.47914
Δ*E* (kcal/mol)	−5.92	−4.26	−4.39	−4.51	−4.06
CP-correction (kcal/mol)	−0.93	−0.80	−0.80	−0.83	−0.35
Δ*E* CP-corrected (kcal/mol)	−4.99	−3.46	−3.59	−3.68	−3.71
			B3LYP/6-31G(d) Coordinates		
monomer	−243.52562	−243.65690	−243.66182	−243.72348	−243.73021
monomer A[a]	−243.52558	−243.65655	−243.66148	−243.72313	−243.72989
monomer A[b]	−243.52644	−243.65731	−243.66224	−243.72395	−243.73028
monomer B[a]	−243.52558	−243.65656	−243.66148	−243.72313	−243.72990
monomer B[b]	−243.52643	−243.65730	−243.66224	−243.72394	−243.73028
dimer (hartree)	−487.06087	−487.32047	−487.33063	−487.45418	−487.46678
Δ*E* (kcal/mol)	−6.05	−4.19	−4.39	−4.53	−3.99
CP-correction (kcal/mol)	−1.08	−0.94	−0.95	−1.03	−0.48
Δ*E* CP-corrected (kcal/mol)	−4.97	−3.25	−3.43	−3.50	−3.51

[a] Monomer energy with dimer geometry and monomer basis. [b] Monomer energy with dimer geometry and dimer basis. Energies in hartrees except as otherwise noted.

Table 6. Binding Energies of the Water Dimer at Different Level Theory (Optimized Calculations)[a]

	AM1	HF/6-31G(d)	B3LYP/6-31G(d)	MP2/6-31G(dp)
monomer	−12.80931	−76.01075	−76.37192	−76.21979
dimer	−25.62733	−152.03046	−152.75596	−152.45080
Δ***E*** (kcal/mol)	−5.46	−5.62	−7.61	−7.05
Δ***E*** CP-corrected (kcal/mol)	N/A	−4.70	−6.84	−5.74

[a] Energies in hartrees except as otherwise noted.

Table 7. Binding Energies of the Water Dimer at Based on Coordinates Obtained by Full Optimization at Four Different Levels of Theory

	HF/6-31G	HF/6-31G(d)	HF/6-31G(d,p)	HF/6-311G(d,p)	HF/6-311+G(d,p)
			AM1 Coordinates		
monomer	−75.98352	−76.01028	−76.02283	−76.04620	−76.05239
monomer A[a]	−75.98341	−76.01019	−76.02272	−76.04608	−76.05227
monomer A[b]	−75.98571	−76.01232	−76.02509	−76.04902	−76.05305
monomer B[a]	−75.98374	−76.01027	−76.02281	−76.04615	−76.05237
monomer B[b]	−75.98496	−76.01155	−76.02419	−76.04784	−76.05268
dimer (hartree)	−151.97218	−152.02163	−152.04623	−152.09342	−152.10253
Δ*E* (kcal/mol)	−3.23	−0.68	−0.36	−0.65	1.41
CP-correction (kcal/mol)	−2.21	−2.14	−2.36	−2.90	−0.69
Δ*E* CP-corrected (kcal/mol)	−1.02	1.46	2.00	2.25	2.10
			HF/6-31G(d) Coordinates		
monomer	−75.98429	−76.01075	−76.02357	−76.04700	−76.05325
monomer A[a]	−75.98430	−76.01072	−76.02352	−76.04693	−76.05318
monomer A[b]	−75.98470	−76.01107	−76.02369	−76.04725	−76.05338
monomer B[a]	−75.98442	−76.01074	−76.02355	−76.04697	−76.05322
monomer B[b]	−75.98565	−76.01187	−76.02496	−76.04900	−76.05397
dimer (hartree)	−151.98031	−152.03046	−152.05597	−152.10284	−152.11387
Δ*E* (kcal/mol)	−7.36	−5.62	−5.54	−5.54	−4.63
CP-correction (kcal/mol)	−1.02	−0.92	−0.99	−1.47	−0.60
Δ*E* CP-corrected (kcal/mol)	−6.34	−4.70	−4.55	−4.06	−4.03
			B3LYP/6-31G(d) Coordinates		
monomer	−75.98324	−76.00975	−76.02216	−76.04546	−76.05167
monomer A[a]	−75.98306	−76.00939	−76.02173	−76.04500	−76.05122
monomer A[b]	−75.98357	−76.00987	−76.02205	−76.04548	−76.05147
monomer B[a]	−75.98326	−76.00963	−76.02201	−76.04529	−76.05151
monomer B[b]	−75.98510	−76.01122	−76.02404	−76.04794	−76.05217
dimer (hartree)	−151.97704	−152.02776	−152.05236	−152.09864	−152.10900
Δ*E* (kcal/mol)	−6.63	−5.18	−5.04	−4.84	−3.55
CP-correction (kcal/mol)	−1.48	−1.30	−1.47	−1.97	−0.57
Δ*E* CP-corrected (kcal/mol)	−5.15	−3.88	−3.57	−2.87	−2.98
			MP2/6-31G(d,p) Coordinates		
monomer	−75.98364	−76.01029	−76.02284	−76.04620	−76.05240
monomer A[a]	−75.98363	−76.01013	−76.02263	−76.04596	−76.05218
monomer A[b]	−75.98407	−76.01053	−76.02286	−76.04635	−76.05242
monomer B[a]	−75.98368	−76.01019	−76.02271	−76.04604	−76.05225
monomer B[b]	−75.98535	−76.01166	−76.02455	−76.04852	−76.05292
dimer (hartree)	−151.97837	−152.02926	−152.05417	−152.10065	−152.11120
Δ*E* (kcal/mol)	−6.96	−5.45	−5.33	−5.18	−4.02
CP-correction (kcal/mol)	−1.32	−1.17	−1.31	−1.81	−0.57
Δ*E* CP-corrected (kcal/mol)	−5.63	−4.28	−4.02	−3.38	−3.45

[a] Monomer energy with dimer geometry and monomer basis. [b] Monomer energy with dimer geometry and dimer basis. Energies in hartrees except as otherwise noted.

reliable structure. The results are included in Table 8. The results reveal that the AMBER geometries are the most inaccurate in both cases by more than an order of magnitude. The AM1 results were much better but (unsurprisingly) not as accurate as those obtained with HF or B3LYP. (AM1+E_{disp})//AM1 is therefore preferred over (AM1+E_{disp})// AMBER.

5. Discussion

The preferred binding sites of the cyclobis(paraquat-*p*-phenylene) ring in the rotaxane and pseudorotaxane systems considered here are known experimentally.[28,30,34,35] We have recovered the same results by carrying out a systematic series of AM1 calculations. In all cases, the lowest energy structures

Table 8. Single-Point Energy Values at the B3LYP/6-311G(dp) Level for the Water and Nitromethane Dimers at Different Optimized Geometries[a]

	energy (hartree)	abs. energy diff. from reported coordinates (hartree)
Nitromethane Dimer		
B3LYP/6-311G(dp)	−489.9393375	0.0033
B3LYP/6-311G(dp)//HF/6-31G(d)	−489.9320871	0.0039
B3LYP/6-311G(dp)//AM1	−489.9298954	0.0061
B3LYP/6-311G(dp)//AMBER	−489.7303006	0.2057
B3LYP/6-311G(dp)// reported_coords	−489.9359884	0
Water Dimer		
B3LYP/6-311G(dp)	−152.8091787	0.0017
B3LYP/6-311G(dp)//HF/6-31G(d)	−152.8073508	0.0001
B3LYP/6-311G(dp)//AM1	−152.8033472	0.0041
B3LYP/6-311G(dp)//AMBER	−152.7967612	0.0107
B3LYP/6-311G(dp)// reported_coords	−152.8074638	0

[a] The absolute difference in energy between each structure and highly accurate published geometries (reported coordinates) are also shown. The reported geometries can be found in the following refs: nitromethane[26,27] and water.[33]

found exhibit ring binding at the experimentally observed binding site positions as shown in Figures 4, 7, and 9. In each system considered, the total energy of the associated complex was found to be lower than that of the dissociated form. This predicts that the components would spontaneously associate in vacuo (and also in a solvent given sufficiently weak solvent effects). This approach to synthesis is referred to as self-assembly and is the preferred synthesis procedure for these systems.[28,30,34,35]

The success of AM1 in making qualitative predictions of binding site preference is notable because $\pi-\pi$ stacking has been assumed to be the dominant intercomponent interaction in these cases and AM1 neglects the dispersion interaction.

The empirical dispersion approximation developed by Grimme[19] was found to be very accurate for estimating the dispersion interaction in several dimer systems. Given this success, it is assumed to provide a reliable description of the intercomponent dispersion interaction in the rotaxane and pseudorotaxane systems. Figures 4 and 9 show that when the contribution of dispersion is added to the AM1 binding energies using the empirical expression of Grimme, the same preferred binding site(s) was predicted as provided by AM1 only. This suggests that inclusion of the dispersion interaction is required for correct quantitative, but not qualitative, description of the intercomponent binding.

To gain insight into *why* the AM1 calculations correctly predict the correct co-conformational preference even though dispersion is neglected, higher order calculations were performed on the pseudorotaxane systems and on the nitromethane and water dimers.

One possible source of the unexpected binding is Basis Set Superposition Error (BSSE). The BSSE is known to artificially increase the predicted strength of binding in nonbonded (van der Waals) complexes because the basis set for the complex is effectively more complete than that for the monomers.[36] While there is no canonical method of correcting for BSSE in an AM1 calculation because there are no standard semiempirical parameters for integrals involving basis functions that are not on atomic centers, the higher order calculations (HF and DFT) allow for the usual CP-correction to be determined. Figure 12 shows the HF/6-31G(d) CP-correction in pseudorotaxane **3** for various positions of the ring relative to the shaft and compares the CP correction to the magnitude of the dispersion interaction as estimated with eq 3. It can be seen that while the CP correction and the dispersion interaction differ significantly in magnitude, they qualitatively track each other very closely. The same result was also found in the nitromethane and water dimers as shown in Figures 14 and 15. Since the BSSE is not corrected for in the AM1 calculation, it makes an artificial contribution to the intercomponent binding, and this contribution has the same qualitative behavior as dispersion. This result, in part, explains why the correct co-conformational preference is recovered with the AM1 method: If dispersion is neglected, then in the absence of other stronger bonding interactions BSSE will lead to a similar structural preference as would the neglected dispersion term.

A second possible reason for the unexpected success of AM1 in predicting co-conformational preference is that van der Waals interactions may not be solely responsible for the binding preference. First, note that our empirical approximation of the electrostatic interaction predicts the correct binding site preference also. (See Figures 6 and 8.) While this empirical approximation to the electrostatic interaction is not quantitatively correct, it does possess the qualitatively correct long-range functional form. This suggests that there is possibly a nondispersive component to the intercomponent binding. Ercolani and Mencarelli[32] computationally studied several pseudorotaxanes, including pseudorotaxane **4**, by performing B3LYP/6-31G(d,p) optimizations and MP2/6-31G(d,p) single-point calculations. They concluded that "face-to-face interactions depend about one-half on electrostatic and frontier orbital contributions (the latter being more important) and the other half on London dispersion forces".[32] On the other hand, they found the edge-to-face interaction to be solely due to dispersion. These results support our finding that dispersion is the dominant intercomponent interaction but is augmented by a nondispersive component. The binding interaction obtained from the empirical dispersion equation greatly exceeds the binding energy determined by AM1 or HF.

A second indication that the intercomponent interaction is not purely due to dispersion comes from the series of first-principles calculations reported in Tables 1−3 (and supported by the results from the calculations on the water and nitromethane dimers reported in Tables 4−6). Table 1 shows the interaction energy ΔE as computed with several levels of theory. (ΔE is defined as the energy of the association reaction: the total energy of the associated complex minus the sum of the total energies of the dissociated components. Therefore, $\Delta E < 0$ implies a bound complex.) The results show that HF/6-31G(d) predicts a negative interaction energy and that there is some residual binding even after application of the CP correction. Since HF neglects dispersion, it is

reasonable to conclude that there is a nondispersive component to the interaction energy. A similar result is obtained at the B3LYP/6-31G(d) level of theory. Since most popular density functionals are local in nature and therefore neglect long-range dispersion,[37] again we can conclude that there is a nondispersive contribution to the intercomponent interaction.

The above conclusion is in some disagreement with the conclusions of a study by Romero et al.,[13] in which they studied pseudorotaxane **4**, among other systems. Romero et al. claimed that "...the origin of stability of cyclobis(paraquat-*p*-phenylene) inclusion complexes with donor molecules is a dispersion interaction which can contribute up to 100% to the binding".[13] To support this claim they conducted DFT optimization calculations using the BHandHLYP/6-31G(d) functional/basis and performed single-point calculations on the resulting structures using both the HF and LMP2 methods with the 6-311+G(d,p) basis (all reported values were CP-corrected). They reported that the HF/6-311+G(d,p)//BH and HLYP/6-31G(d) calculation on pseudorotaxane **4** reveals a repulsive interaction. Their interpretation is that, since the interaction is attractive ($\Delta E < 0$) at the DFT and MP2 levels but becomes repulsive ($\Delta E > 0$) when the strictly nondispersive HF method is applied to the same structure, the entire binding must result from dispersion interactions. By contrast, we show in Table 2 that the binding is still attractive when HF single-point calculations are carried out on a variety of geometries. Exact coordinates for the structures of Romero et al.[13] were not published, but we found $\Delta E < 0$ for HF−SP calculations carried out with five different basis sets on structures obtained by full optimization at four different levels of theory.

There are at least two indications that pseudorotaxane **4** possesses a nondispersive component to the intercomponent interaction, despite the interpretation of Romero et al.[13] First, the fact $\Delta E < 0$ is predicted at the BH and HLYP/6-31G(d) level of theory indicates that there is a nondispersive component to the intercomponent interaction. Since this interaction is a nonbonding (van der Waals) interaction, it occurs on length scales that are generally longer than the local interaction included in most common density functionals.[37,38] Second, we show in Table 3 that the difference in energy between a fully optimized structure and a single-point calculation based on a structure that was optimized at a different level of theory is significant in all cases considered, in some cases larger than the obtained binding energy. Error occurs in both the components and the system, and often these errors cancel each other out, but reliable prediction of the binding energy relies on such fortuitous cancellation of errors.

6. Conclusions

The AM1 Hamiltonian is computationally efficient yet incorporates an explicit description of the electronic structure of a system. These features render it attractive for application to large systems where multiple charge and electronic states must be considered, as is the case for switchable rotaxanes and pseudorotaxanes. Many rotaxanes exhibit $\pi-\pi$ stacking interactions between the ring and the binding stations on the shaft. $\pi-\pi$ stacking results from dispersion forces. Unfortunately, since AM1 is a HF-based technique, AM1 calculations neglect dispersion. Remarkably, AM1 calculations often still recover the correct binding site preference. We have discovered that this is in part due to basis set superposition error (BSSE). Typically one corrects for BSSE in an intermolecular interaction using the counterpoise (CP) correction, but there is no canonical way to perform the CP correction in an AM1 calculation. AM1 calculations of intercomponent interactions therefore include BSSE. We have shown that the BSSE qualitatively mimics the dispersion that is neglected in the AM1 calculation. While the magnitude of the intercomponent binding is not properly "predicted" by the BSSE, qualitatively correct binding site preference can result. Clearly, this is a theoretically unreliable way to predict the structures of interlocked macromolecular complexes where dispersion dominates the intercomponent interaction. AM1 is more defensible as a technique to model interlocked macromolecular complexes where hydrogen-bonding governs the intercomponent interaction, because AM1 is known to predict qualitatively correct trends among hydrogen-bonding interactions.[14]

This research was supported by National Science Foundation grant CHE0449595 and DuPont Inc.

References

(1) Wenz, G.; Han, B.-H.; Muller, A. Cyclodextrin Rotaxanes and Ployrotaxanes. *Chem. Rev.* **2006**, *106*, 782−817.

(2) Credi, A. Artificial nanomachines based on interlocked molecules. *J. Phys.: Condens. Matter* **2006**, *18*, 1779−1795.

(3) Tian, H.; Wang, Q.-C. Recent progress on switchable rotaxanes. *Chem. Soc. Rev.* **2006**, *35*, 361−374.

(4) Frankfort, L.; Zheng, X.; Sohlberg, K. Mechanical Molecular Nanodevices. *Encycl. Nanosci. Nanotech.* **2004**, *5*, 73−89.

(5) Sohlberg, K.; Lee, K.-H. An introduction to modeling interlocked molecule systems and application to a "molecular elevator". *J. Comput. Theor. Nanosci.* **2006**, *3* (6), 865−873.

(6) Dewar, M. J. S.; Zoebisch, E. G.; Healy, E. F.; Stewart, J. J. P. AM1: A new general purpose quantum mechanical molecular model. *J. Am. Chem. Soc.* **1985**, *107*, 3902.

(7) de Federico, M.; Jaime, C.; Free Energy Calculations (FEP and TI): Conformational Preference of a Cyclodextrinic [2]Catenane: A Case Study. *J. Comput. Theor. Nanosci.* **2006**, *3* (6), 874−879.

(8) Shirts, R. B.; Stolworthy, L. D. Conformational Sensitivity of Polyether Macrocycles to Electrostatic Potential: Partial Atomic Charges, Molecular Mechanics, and Conformational Predictions. *J. Inclusion Phenom.* **1995**, *20*, 297−321.

(9) Rappe, A. K.; Goddard, W. A, III. Charge equilibration for molecular dynamics simulations. *J. Phys. Chem* **1991**, *95*, 3358−3363.

(10) Zheng, X.; Sohlberg, K. Origin of Co-Conformational Selectivity in a [3]rotaxane. *J. Phys. Chem. A* **2006**.

(11) Grabuleda, X.; Ivanov, P.; Jaime, C. Shuttling Process in [2]Rotaxanes. Modeling by Molecular Dynamics and Free Energy Perturbation Simulations. *J. Phys. Chem. B* **2003**, *31*, 7582−7588.

(12) Grabuleda, X.; Jaime, C. Molecular Shuttles. A Computational Study (MM and MD) on the Translational Isomerism in Some [2] Rotaxanes. *J. Org. Chem.* **1998**, *63*, 9635−9643.

(13) Romero, C.; Fomina, L.; Fomine, S. How Important Is the Dispersion Interaction for Cyclobis(paraquat-pphenylene)-Based Molecular "Shuttles"? A Theoretical Study. *Int. J. Quantum Chem.* **2005**, 102.

(14) Buemi, G.; Zuccarello, F.; Raudino, A. Hydrogen bonding and rotation barriers: A comparison between MNDO and AM1 results. *J. Mol. Struct. THEOCHEM* **1988**, *164* (3−4), 379−389.

(15) Frankfort, L.; Sohlberg, K. Semiempirical study of a pH-switchable [2]-rotaxane. *J. Mol. Struct. THEOCHEM* **2003**, *621*, 253−260.

(16) Zheng, X.; Sohlberg, K. Modeling of a Rotaxane-based Molecular Device. *J. Phys. Chem.* **2003**, *107*, 1207.

(17) Zheng, X.; Sohlberg, K. Modeling bistability and switching in a [2]catenane. *Phys. Chem. Chem. Phys.* **2004**, *6*, 809 - 815.

(18) Schmidt, M. W.; Baldridge, K. K.; Boatz, J. A.; Elbert, S. T.; Gordon, M. S.; Jensen, J. H.; Koseki, S.; Matsunaga, N.; Nguyen, K. A.; Su, S.; Windus, T. L.; Dupuis, M.; Montgomery, J. A. General Atomic and Molecular Electronic Structure System. *J. Comput. Chem.* **1993**, *14*, 1347−1363.

(19) Grimme, S. Semiempirical GGA-Type Density Functional Constructed with a Long-Range Dispersion Correction. *J. Comput. Chem.* **2006**, *27* (15), 1787−1799.

(20) Weiner, S. J.; Kollman, P. A.; Case, D. A.; Singh, V. C.; Ghio, G.; Alagona, G.; Profeta, S., Jr.; Weiner, P. A new force field for molecular mechanical simulation of nucleic acids and proteins. *J. Am. Chem. Soc.* **1984**, *106*, 765−784.

(21) Hyperchem. *Hyperchem, Release 5.01 for Windows*; Hypercube Inc.: 419 Phillip Street, W., Ontario N2L3X2, Canada, 1996.

(22) Flükiger, P. H. P. L.; Portmann, S.; Weber, J. *MOLEKEL 4.0*; 2000.

(23) Diep, P.; Johnsona, J. K. An accurate H2−H2 interaction potential from first principles. *J. Chem. Phys.* **2000**, *112* (10), 4465−4473.

(24) Aquilanti, V.; Bartolomei, M.; Cappelletti, D.; Carmona-Novillo, E.; Pirani, F. The N2−N2 system: An experimental potential energy surface and calculated rotovibrational levels of the molecular nitrogen dimer. *J. Chem. Phys.* **2002**, *117* (2), 615−627.

(25) Rybak, S.; Jeziorski, B.; Szalewicz, K. Many-body symmetry-adapted perturbation theory of intermolecular interactions. H20 and HF dimers. *J. Chem. Phys.* **1991**, *95* (9), 6576−6601.

(26) Cole, S. J.; Szalewicz, K. Correlated calculation of the interaction in the nitromethane dimer. *J. Chem. Phys.* **1986**, *84* (12), 6833−6836.

(27) Cole, S. J.; Szalewicz, K.; Bartlett, R. J. Nitromethane Dimer Potential Energy Surface Studies. *Int. J. Quantum Chem.* **1986**, *30*, 695−711.

(28) Anelli, P. L.; Spencer, N.; Stoddart, J. F. A molecular shuttle. *J. Am. Chem. Soc.* **1991**, *113*, 5131.

(29) Levine, I. N. Comparisons of Methods. In *Quantum Chemistry*, 4th ed.; Prentice Hall: Englewood Cliffs, NJ, 1991; pp 594−607.

(30) Córdova, E.; Bissel, R. A.; Spencer, N.; Ashton, P. R.; Stoddart, J. F.; Kaifer, A. E. Novel Rotaxanes Based on the Inclusion Complexation of Biphenyl Guests by Cyclobis-(paraquat-*p*-phenylene). *J. Org. Chem.* **1993**, *58*, 6550−6552.

(31) Bissell, R. A.; Cordova, E.; Kaifer, A. E.; Stoddart, J. F. A Chemically and Electrochemically Switchable Molecular Shuttle. *Nature* **1994**, *369*, (6476), 133−137.

(32) Ercolani, G.; Mencarelli, P. Role of Face-to-Face and Edge-to-FaceAromatic Interactions in the Inclusion Complexation of Cyclobis(paraquat-p-phenylene): A Theoretical Study. *J. Org. Chem.* **2003**, *68*, 6470−6473.

(33) Szalewicz, K.; Cole, S. J.; Kolos, W.; Bartlett, R. J. A Theoretical Study of the Water Dimer Interaction. *J. Chem. Phys.* **1988**, *89*, 3662−3673.

(34) Anelli, P. L.; Ashton, P. R.; Ballardini, R.; Balzani, V.; Delgado, M.; Gandolfi, M. T.; Goodnow, T. T.; Kaifer, A. E.; Philp, D.; Pietraszkiewicz, M.; Prodi, L.; Reddington, M. V.; Slawin, A. M. Z.; Spencer, N.; Stoddart, J. F.; Vicent, C.; Williams, D. J. Molecular Meccano. 1. [2]Rotaxanes and a [2]Catenane Made to Order. *J. Am. Chem. Soc.* **1992**, *114* (1), 193−218.

(35) Ballardini, R.; Balzani, V.; Gandolfi, M. T.; Prodi, L.; Venturi, M.; Philp, D.; Ricketts, H. G.; Stoddaart, J. F. A photochemically driven molecular machine. *Angew. Chem., Int. Ed. Engl.* **1993**, *32*, 1301−1302.

(36) Clark, T. Ab Initio Methods. In *A Handbook of Computational Chemistry*; Wiley: New York, 1985; pp 233−317.

(37) Gerber, I. C.; Ángyán, J. G. London dispersion forces by range-separated hybrid density functional with second order perturbational corrections: The case of rare gas complexes. *J. Chem. Phys.* **2007**, *126* (044103), 1−14.

(38) Podeszwa, R.; Bukowski, R.; Szalewicz, K. Potential Energy Surface for the Benzene Dimer and Perturbational Analysis of π-π Interactions. *J. Phys. Chem. A* **2006**, *110*, 10345−10354.

CT7001623